JETIR.ORG ISSN: 2349-5162 | ESTD Year : 2014 | Monthly Issue
JOURNAL OF EMERGING TECHNOLOGIES AND INNOVATIVE RESEARCH (JETIR)
An International Scholarly Open Access, Peer-reviewed, Refereed Journal

EXPLORING MOLECULAR PROPERTIES OF A NOVEL BENZOFURAN DERIVATIVE USING DENSITY FUNCTIONAL THEORY

[1]Annoji Reddy R., *[2]Ravikantha M. N., [3]Hanumanagoud H

[1]Assistant Professor, Department of Physics, GVVP Govt. First Grade College, Hagaribommana Halli – 583 212, India.,
[2]Assistant Professor, Department of Physics, Government Science College, Chitradurga - 577 501, Karnataka, India.
[3]Lecturer In Chemistry, Department of Chemistry, K.L.E. Society's P.C.Jabin Science College, Hubli – 580 031, India.

Abstract: In the present work, several molecular properties of a novel benzofuran derivative; 7-methoxy-benzofuran-2-carboxylic acid (7MBC) were explored computationally from density functional theory (DFT) techniques embedded the Gaussian software using hybrid exchange-Correlation function, B3LYP with 6311+(d,p) basis set. The reported harmonic wavenumbers are in excellent agreement with the experimental FT-IR values. Molecular properties such as FMO, GRDs and MEP are explored to understand the chemical reactivity of the given molecule. the HOMO–LUMO energy gap (4.189 eV) suggest higher polarizability and hence this benzofuran derivative is expected to be soft as well as reactive and have favorable NLO futures. NLO properties such as polarizability, first and second order static hyperpolarizability were evaluated to explore the probable NLO applications.

Keywords: Benzofuran, DFT, FMO, MEP, NLO

I. INTRODUCTION

Benzofurans are interested and vital class among heterocyclic compounds, usually recognized as heterocyclic analog of naphthalene. Numerous biologically active benzofurans have been isolated from a large range of natural products such as medicinal plants and seafood, as well as from bacterial or fungal metabolites.

The structures containing benzofuran-carboxylic acid are known for exhibiting wide gamma of biological activities. These derivatives were found to be antagonists[1], anti-inflammatory agents[2], and local anesthetics[3], antimicrobial agents[4], cardiovascular agents[5] and antibacterial agents[6]. Variously substituted 2-benzofurancarboxylic acid derivatives show selective cytotoxicity against human cancer cell line[7]. Amide derivatives of halo-benzofuran-2- carboxylic acid were used in the treatment of neural diseases[8]. The antibacterial, antifungal activity and DNA cleavage study of derivatives incorporating benzofuran moiety were reported[9]. Further, Conjugated heterocyclic rings exhibit an significant role in organic LEDs due to their hole-transporting material properties[10]. Fluoreno benzofuran is used as high triplet energy host material in the synthesis of green phosphorescent OLEDs[11,12].

Owing to these significant applications, benzofuran-2-carboxylic acid derivatives have been the subject of theoretical and experimental studies. The reports of experimental and quantum computational investigations on structural, spectroscopic, various physiochemical, optical and thermal properties, chemical reactivity and molecular docking activities of some benzofuran carboxylic acid derivatives were found in the literature[13–15].

To the best of our knowledge, the detailed literature review reveals that there have been no experimental and theoretical studies reported on molecular properties of the selected derivatives with benzofuran-2-carboxylic acid structure. This inadequacy in the literature encouraged us to take up the present work. In the existing effort, the geometrical optimization, spectroscopy (FT-IR), Several molecular properties of the title molecule were analysed using experimental spectroscopic and theoretical DFT methods.

II. COMPUTATIONAL METHODS

The initial geometry of the proposed molecule; 7-methoxy-benzofuran-2-carboxylic acid [7MBC] was taken from the work reported by the one of the co-authors, Hanumanagoud et al[9].

2.1. Spectral Techniques

The room temperature Fourier transform infrared (FTIR) spectrum of the molecules was recorded using KBr pellets on Nicolet Impact 410 FT-IR spectrometer, in the range 4000 - 400 cm^{-1}. The ^1H NMR spectra were recorded on Bruker AM-400 MHz NMR Spectrometer using $CDCl_3$ as solvent with Tetramethyl silane (TMS) as an internal standard. Chemical shifts are reported in ppm (δ).

2.2. Computational Techniques

The optimization of geometry and subsequent calculations were carried out employing DFT- B3LYP functional method with 6-311+G (d, p) basis set. For each structure, molecular geometry was fully optimized in gas phase in Gaussian 09: IA32W-G09RevC.01 quantum computational package[16]. The molecular simulations, graphical presentations and analysis of the Gaussian output were performed using Gauss View 6.0.16 molecular visualization software[17].

Optimized structures are used in the vibrational frequency calculations to ensure that the obtained structures represent a local minimum. The theoretically generated vibrational spectrum is interpreted through the Potential Energy Distribution (PED) using Vibrational Energy Distribution Analysis (VEDA) program[18]. The streamlined analysis of MEP and FMO were carried out and HOMO-LUMO energies and Global reactivity descriptors[19] are proposed. Using the optimized coordinates, the first and second static hyperpolarizabilities were calculated by the finite field perturbation method in order find the potential of title molecules as good NLO candidates.

2.3 Preparation

The careful hydrolysis of 7-methoxy-benzofuran-2-carboxylic acid ethyl ester in ethanolic potassium hydroxide solution gives carboxylic acid

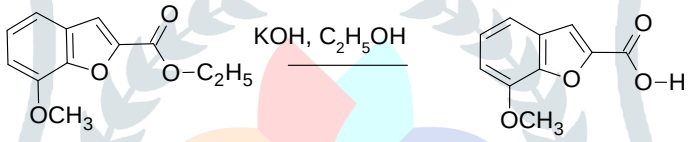

To a solution of 7-methoxy-benzofuran-2-carboxylic acid ethyl ester (0.02 mol) in absolute ethanol (30 mL), ethanolic potassium hydroxide (2 g in 20 mL absolute ethanol) was added and the reaction mixture was heated under reflux for 2 h on a water bath. The excess of ethanol was distilled off under reduced pressure and the residual solution was diluted with cold water. The clear solution thus obtained was cooled and acidified with dilute hydrochloric acid carefully to precipitate the carboxylic acid. It was collected, washed with water and crystallized from a mixture of benzene and petroleum ether as colourless needles. Yield 88%, melting point 205 oC. Calculated : C (62.50), H (4.20), Found: C (62.65), H (3.00), N(4.21)

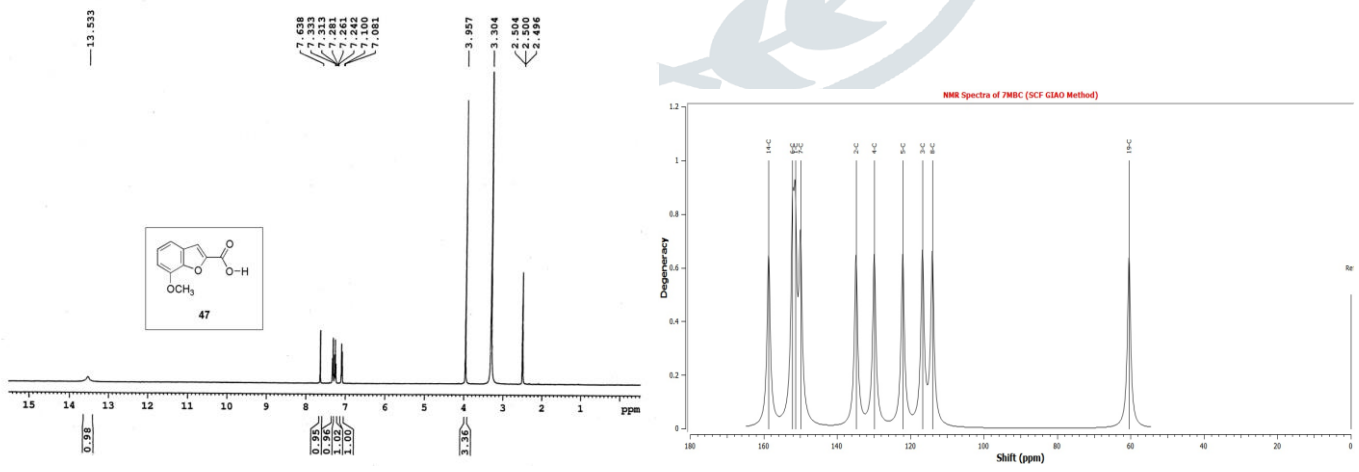

Figure 1: The experimental and theoretical 1H NMR spectra of 7MBC molecule.

To provide additional evidence for the proposed structure, the 1H NMR and mass spectrum of 7MBC were recorded. The 1H NMR spectrum in DMSO-d6 was exhibited a singlet at 3.95 ppm due to OCH3 protons, a multiplet in the range of 7.08-7.33 ppm were due to the C4-C6 aromatic protons and a singlet was observed at 7.63 ppm due to C3-H. The carboxylic acid proton was resonated as a singlet at 13.53 ppm. The molecular ion peak was observed at m/z 192 confirmed the formation of 7MBC.

III. Results And Discussion

3.1 Optimized Molecular Geometry

The given geometrical structure belongs C1 point group. Optimized bond lengths, bond angles and torsional angles of 7MBC computed using the DFT method are portrayed in Table 1 and atomic numbering scheme of 7MBC molecule obtained by DFT computation is exhibited in Fig. 2. The 7MBC are listed Table 1.

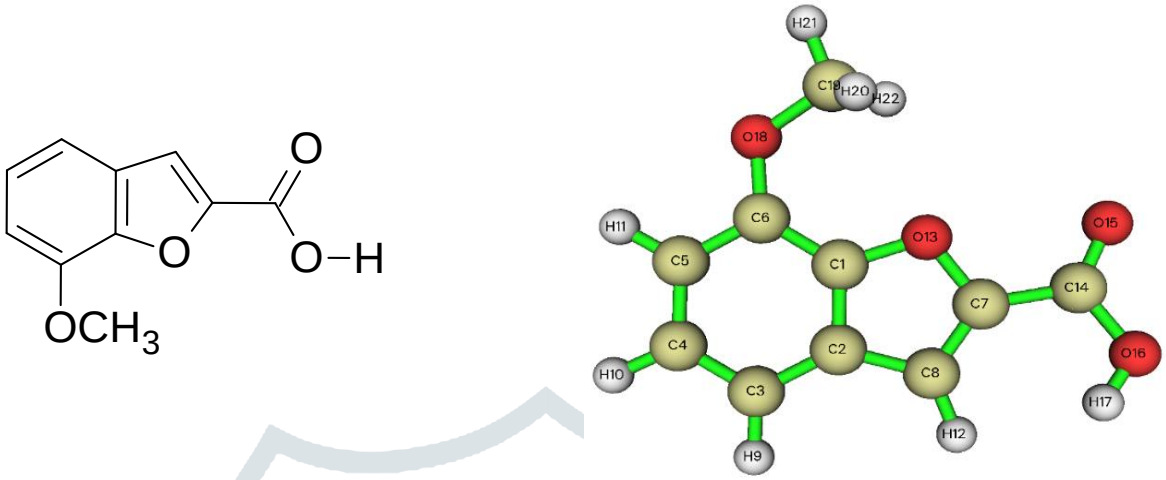

Figure 2: The molecular structure and ground state optimized geometry of 7MBC with numeration scheme for atoms computed at DFT-B3LYP/6-311+G(d,p) level of theory.

Bond lengths. From Table 1, it is found that for 7MBC geometry, the shortest (strongest) bond is found to be O_{16}-H_{17} ≈0.9648 Å in the carboxylic acid fragment and the longest (weakest) is C_7-C_{14}≈1.513 Å linked with furan ring and carboxylic acid fragment. The lower value of O-H bond shows its greater tendency to form cation and leads to displacement of –COOH group. The resonating C≃C double bonds are shortened in length and also stronger than single bonds. The deviations are also correlated with the effect of electron donating substituents on the ring.

Table 1. Selected geometrical parameters of 7MBC

Bond Lengths (in Å)			Bond Angles (in °)					
Name	**Definition**	**Value**	**Name**	**Definition**	**Value**	**Name**	**Definition**	**Value**
R1	R(C1,C2)	1.4085	A1	A(C1,C2,C3)	120.54	A18	A(4C,5C,11H)	120.43
R2	R(C2,C3)	1.4018	A2	A(2C,3C,4C)	117.21	A19	A(6C,5C,11H)	117.26
R3	R(C3,C4)	1.3866	A3	A(3C,4C,5C)	121.71	A20	A(1C,6C,18O)	127.10
R4	R(C4,C5)	1.4026	A4	A(4C,5C,6C)	122.31	A21	A(5C,6C,18O)	117.33
R5	R(C5,C6)	1.3962	A5	A(1C,6C,5C)	115.55	A22	A(8C,7C,14C)	133.22
R6	R(C6,C1)	1.4022	A6	A(C2,C1,C6)	122.66	A23	A(13O,7C,14C)	115.46
R7	R(C3,H9)	1.0827	A7	A(C2,C1,13O)	110.28	A24	A(2C,8C,12H)	126.09
R8	R(C4,H10)	1.0838	A8	A(C1,C2,C8)	104.95	A25	A(7C,8C,12H)	127.08
R9	R(C5,11H)	1.0833	A9	A(8C,7C,13O)	111.30	A26	A(7C,14C,15O)	123.84
R10	R(C7,13O)	1.3685	A10	A(2C,8C,7C)	106.82	A27	A(7C,14C,16O)	115.41
R11	R(C1,O13)	1.368	A11	A(1C,13O,7C)	106.64	A28	A(15O,14C,16O)	120.74
R12	R(C2,C8)	1.4359	A12	A(C6,C1,13O)	127.05	A29	A(14C,16O,17H)	111.19
R13	R(C7,C8)	1.3637	A13	A(3C,2C,8C)	134.49	A30	A(C6C,18O,19C)	120.22
R14	R(C8, H12)	1.0799	A14	A(2C,3C,9H)	121.29	A31	A(18O,19C,20H)	110.87
R15	R(C7, C14)	1.4788	A15	A(4C,3C,9H)	121.49	A32	A(18O,19C,21H)	105.08
R16	R(C6,18O)	1.3549	A16	A(3C,4C,10H)	119.76	A33	A(18O,19C,22H)	111.57
R17	R(14C,15O)	1.1993	A17	A(5C,4C,10H)	118.52	A34	A(20H,19C,21H)	109.67
R18	R(14C,16O)	1.3611				A35	A(20H,19C,22H)	109.61
R19	R(16O,17H)	0.9648				A36	A(21H,19C,22H)	109.95
R20	R(18O,19C)	1.4356						
R21	R(19C,20H)	1.0928						
R22	R(19C,21H)	1.0884						
R23	R(19C,22H)	1.0903						

3.2 Spectroscopy

The title compound comprises of 22 atoms; accordingly, it has 60 fundamental vibrational modes are observed under C1 point group. In the present investigation, the experimental IR spectrum contained a broad band in the region of 3400-2525 cm^{-1} and sharp band at 1690 cm^{-1} due to carboxylic acid OH and C=O group frequencies respectively as shown in fig.3. The spectroscopic mark of 7MBC has been examined by the hypothetical FT-IR spectra using B3LYP/6311+G(d,p) level of DFT Theory and compared with experimental data as shown in Table 2.. A good correlation was found between observed and calculated values.

Table 2: The experimental (FT-IR) and computed values of wavenumbers, Vibrational Temperatures , Reduced Mass and Force constants of 7MBC using DFT-B3LYP/6311+G(d,p).

Normal Modes	Experimental Wavenumber	Harmonic Wavenumber (cm-1)	Vibrational Temperatures (Kelvin)	Reduced Mass (a.u)	Force constant (mDyne/A)	IR Intensity (KM/Mole)
1	3404	3812	5484.82	1.07	9.13	29.26
2		3230	4647.89	1.10	6.75	3.34
3		3200	4604.57	1.10	6.61	6.69
4	3136	3194	4594.91	1.09	6.56	5.95
5		3176	4569.97	1.09	6.46	5.75
6	2982	3146	4526.45	1.11	6.45	17.29
7	2915	3116	2357.03	1.10	6.31	22.25
8	2846	3038	2347.40	1.03	5.62	38.43
9	1690	1825	2290.34	11.00	21.58	454.44
10	1621	1638	4483.11	8.16	12.91	24.01
11	1588	1632	4371.34	6.58	10.32	87.25
12	1572	1592	2626.21	6.29	9.39	77.94
13		1519	2185.83	2.81	3.82	83.43
14		1502	2160.57	1.05	1.40	21.47
15	1492	1494	2150.20	1.05	1.38	18.21
16	1462	1478	2126.88	1.25	1.61	17.32
17	1424	1440	2072.44	2.98	3.65	15.39
18	1362	1385	1992.59	7.78	8.79	29.44
19	1330	1351	1944.28	4.64	4.99	188.63
20		1321	1900.95	4.49	4.62	203.08
21	1270	1298	1867.01	2.20	2.18	144.63
22		1250	1798.75	2.08	1.91	170.46
23	1227	1237	1780.36	2.09	1.89	133.69
24	1207	1208	1738.47	2.05	1.76	37.14
25	1185	1188	1709.91	1.23	1.03	7.66
26		1167	1678.48	1.30	1.05	3.95
27	1154	1164	1674.54	1.51	1.21	33.10
28		1105	1590.00	2.54	1.83	83.91
29	1094	1100	1583.05	3.20	2.28	88.68
30	1068	1073	1544.22	2.10	1.42	11.99
31	975	1002	1442.23	6.51	3.85	22.41
32	941	976	1404.03	1.29	0.72	0.53
33	901	959	1380.10	8.95	4.85	5.39
34		893	1284.15	1.43	0.67	0.30
35	853	869	1250.34	6.21	2.76	10.98
36		836	1203.28	1.64	0.68	36.57
37	784	787	1132.89	2.14	0.78	29.90
38		758	1090.43	3.45	1.17	6.78
39	734	753	1083.87	4.62	1.55	14.44
40		735	1057.38	2.72	0.86	39.53
41	696	671	965.31	6.50	1.72	2.46
42	627	629	904.62	5.20	1.21	3.63
43		615	884.18	5.11	1.14	0.83
44	579	586	843.65	5.20	1.05	2.57
45	536	570	819.74	5.58	1.07	1.88
46		551	792.36	4.11	0.73	0.91
47		513	738.28	6.99	1.08	0.39
48		458	659.52	5.10	0.63	4.97
49		409	587.78	1.22	0.12	88.48
50		373	536.49	6.73	0.55	8.54
51		321	461.31	5.11	0.31	8.81
52		296	425.23	4.62	0.24	2.64
53		254	364.81	5.04	0.19	5.81
54		231	332.23	2.48	0.08	1.08
55		212	304.45	2.09	0.06	1.73
56		161	231.69	2.25	0.03	0.55
57		119	171.68	5.99	0.05	7.26
58		92	132.96	7.56	0.04	0.44
59		40	57.25	5.52	0.01	4.71
60		30	43.32	3.05	0.00	10.98

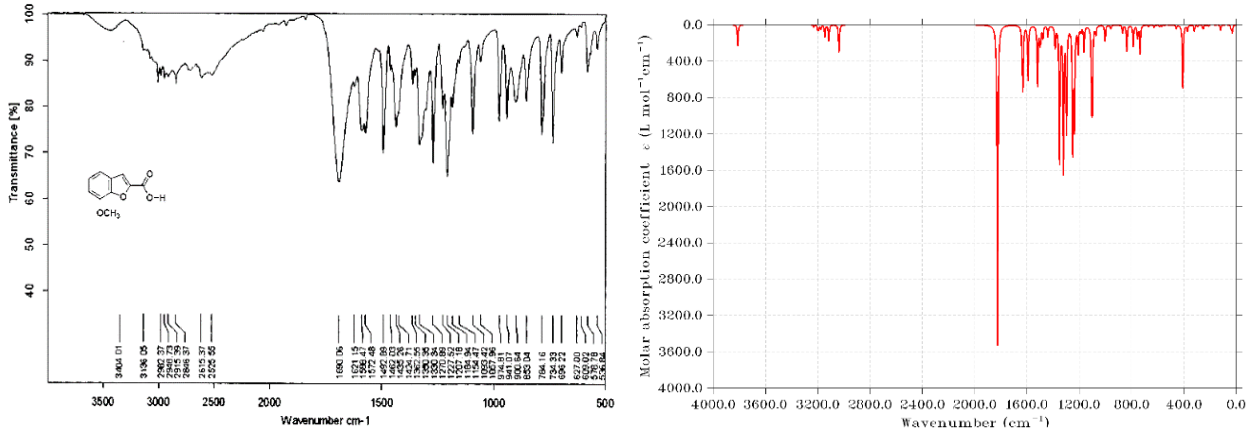

Figure 3: The experimental (left) and hypothetical FT-IR spectra (right) using B3LYP/6311+G(d,p) level of DFT Theory.

3.3 Frontier Molecular Orbitals

The highest occupied molecular orbital (HOMO) and lowest unoccupied molecular orbital (LUMO) together constitute the Frontier Molecular Orbital (FMO). The Frontier Molecular Orbital (FMO) has a greater impact on the reaction sensitivity or chemical stability, electrical transport properties and optical properties of the molecule[20–22].

The FMO Analysis of 7MBC molecule with B3LYP techniques with 6-311G+(d,p) premise set predicts 50 occupied molecular orbitals and 304 vacant molecular orbitals. The iso-density portraits for the HOMO and LUMO are as depicted in the fig. (). The red and green colors of the MO plot represent the positive and negative phase of the molecule respectively. From the portraits of FMOs in Fig.4., it is clear that the electron densities of HOMO–2 are mainly localized on the carboxyl group of the molecule. HOMO–1 is localized on the benzofuran ring, Oxygen attached to C6 and C=O, and HOMO is mainly localized on benzofuran ring, Oxygen attached to C6 and methyl group of 7MBC molecule. The electron densities of LUMO are localized on the benzofuran ring, Oxygen attached to C6 and carboxyl group. LUMO+1 mainly localized carboxyl group and LUMO+2 is mainly localized on the benzene ring and Oxygen in the furan ring of 7MBC molecule. HOMO and LUMO show π and σ bond characteristics respectively.

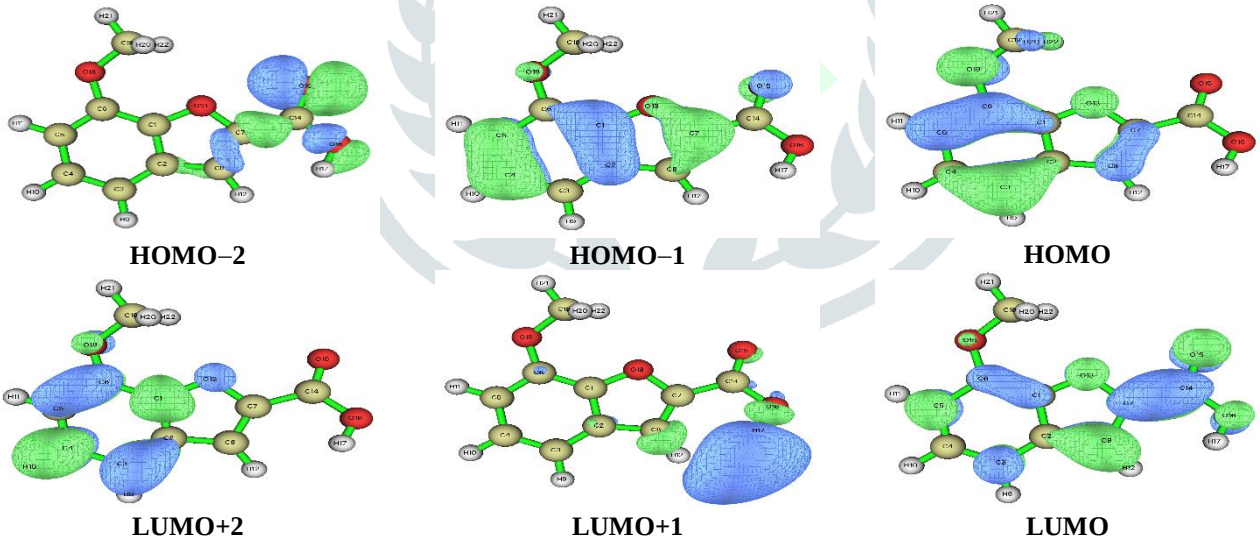

Figure 4:The atomic orbital compositions of the frontier molecular orbitals /Distribution of electron densities in the FMOs.

Further, Interaction between HOMO and LUMO orbitals is responsible for the progression of electron transport in the molecular system[23]. From the FMO analysis, it has been observed that there is intra-molecular charge transfer from the electron donating group (Methoxy group) to the electron accepting (carboxyl group) through the π-conjugation system which leads to the molecular stability.

Besides considering charge transfer within the molecule, The HOMO and LUMO energies are determined and an energy barrier ΔE = 0.154 (a.u) =4.189 eV was recognized between the HOMO and LUMO orbitals. The values of all FMO energy parameters are introduced in Table 3. The lower value for the HOMO–LUMO energy gap in indicated that the eventual energy transfer interactions took place within the molecule[24]. The small energy gap also indicates high polarizability and hence this benzofuran derivative is expected to be soft as well as reactive[25].

Table 3: Frontier Molecular Orbital Energies				
FMO	H-L Energy Gap			
	(a.u)		(eV)	
HOMO	-0.235	0.154	-6.388	4.190
LUMO	-0.081		-2.198	
HOMO-1	-0.264	0.238	-7.176	6.478
LUMO+1	-0.026		-0.697	
HOMO-**2**	-0.303	0.286	-8.232	7.777
LUMO+**2**	-0.017		-0.455	

3.4 Global Reactivity Descriptors (GRDs)

In order to comprehend various aspects of pharmacological sciences comprising drug design and possible eco-toxicological characteristics of drug molecules, several new chemical reactivity descriptors have been proposed. The chemical reactivity of molecular species as a whole can be predicted conceptually using first principles of DFT technique in terms few global indices termed as global reactivity descriptors (GRDs)[26] which include electro negativity (χ), chemical potential (μ), global hardness (η), global softness (ν) and electrophilicity index (ω).

In the present work, the global indices of the title molecule were computed using the Equations discussed elsewhere[23] based on Koopmans' hypothesis and presented in Table 4.

Table 4:Calculated Global Reactivity Descriptors# of 7MBC using B3LYP/6-311 G + (d, p) basis set.

The quantum chemical parameters	Calculated value (a.u)	Calculated value (eV)
Ionization Potential (I)	0.235	6.388
Electron Affinity (A)	0.081	2.198
Electronegativity (χ)	0.158	4.293
Chemical Potential (μ)	-0.158	-4.293
Hardness(η)	0.077	2.095
Softness (σ) (eV^{-1})	6.494	0.239
Electrophilicity Index (ω)	0.162	4.398
Electron accepting power (w^{+})	0.092	2.514
Electron donating power (w^{-})	0.250	6.807
Additional electronic charge (ΔN_{max})	2.049	2.049

#all values are in hatree/eV except for ν, which is in $hatree^{-1}/eV^{-1}$ and W^{-} and W^{+} are ratios

3.4 MEP Analysis

The molecular electrostatic potential (MEP) serves as a useful quantity to explain hydrogen bonding, reactivity and structure activity relationship of molecules including biomolecules and drugs. Electrostatic potential surfaces correlate with the dipole moment, electronegativity, partial charges and site of chemical reactivity of the molecule. The MEP has been used for predicting sites and relative reactivity towards electrophilic attack and in studies of biological recognition and hydrogen bonding interactions.

The quantitative analysis of MESP of the titled molecules have been performed using LIBRETA, the ESP evaluation code[27–29] embedded in multiwfn 3.8.1 program[30] with a cubic grid spacing of 0.25 a.u. (0.1323 Å) and visual graphics displayed in Fig 3 are rendered by the VMD 1.9.1 program[31] with the BWR colour scaling scheme which represents the regions of highest repulsive potential appear in red and those of highest attractive potential appear in blue.

The fig.5a delineates the molecular electrostatic surface of 7MBC. the red and blue spots over the surface refer to points of local maximum and minimum of ESP respectively. The quantitative analysis of the molecular surface[28,29] and the properties of ESP[32] are depicted in the Table 5. From the table, it is seen that, there are 11 minima and 4 maxima with Global surface minimum of -38.753 **k**cal/mol and Global surface maximum of 60.414 **k**cal/mol.

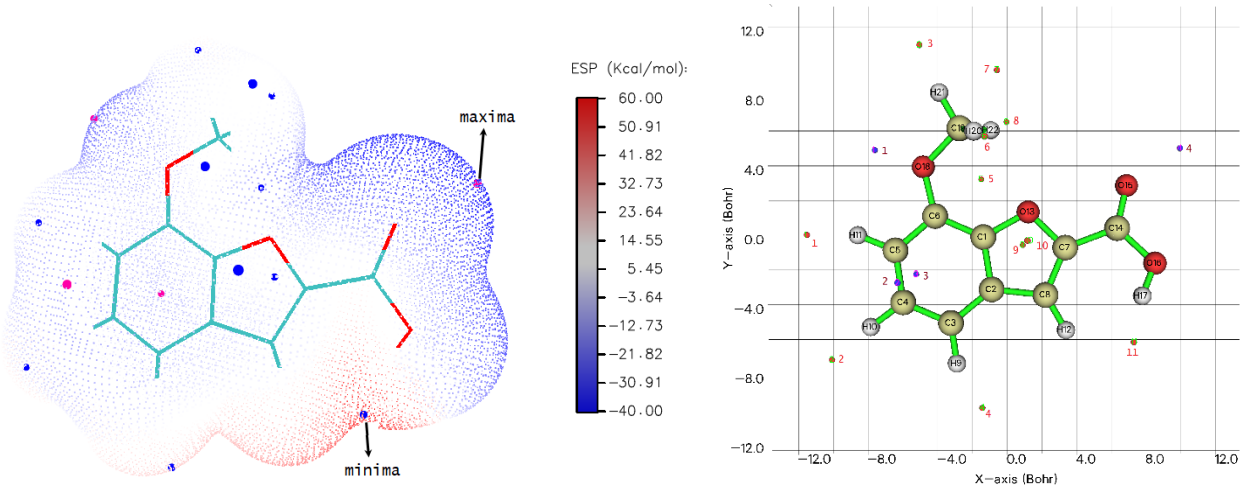

Figure 5:Visual representation of MEP values at different local VdW surfaces of (a) Acetaminophen and (b) Diclofenac estimated at B3LYP level of theory

The positions local surface maxima and minima are shown in the Table 5 and Fig 5b. As seen from these, it is clear that for ACE molecule, the global minimum ie., The strongly negative electrostatic potential (-38.753 kcal/mol) is visible over the lone- pair regions close to O_{15} atom of the carboxyl group acts as a potential site for the electrophilic attack. The very strongly positive electrostatic potential ($V_{S,max} \approx +60.414$ kcal/mol) is localized near the hydrogen atom (H_{17}) of the carboxyl group. Fig. 6 represents the polar surface area as a function of ESP. from the figure, it is seen that the molecule is slightly polar.

Table 5: Properties on the Molecular Electrostatic Surface

Property of ESP	**Value**
Number of surface minima	4
Global surface minimum (kcal/mol):	-38.753
Number of surface maxima	11
Global surface maximum (kcal/mol):	60.414
Overall surface area ($Å^2$)	218.24
Positive surface area ($Å^2$)	130.84
Negative surface area ($Å^2$)	87.402
Total ESP variance (σ^2_{total})(kcal/mol)^2	251.275
Degree of charge balance (ν):	0.2488
Internal charge separation (π): (kcal/mol)	13.05479
Molecular polarity index(kcal/mol)	13.36285
Nonpolar surface area (|ESP| <= 10 kcal/mol):	49.01 %
Polar surface area (|ESP| > 10 kcal/mol):	50.99 %

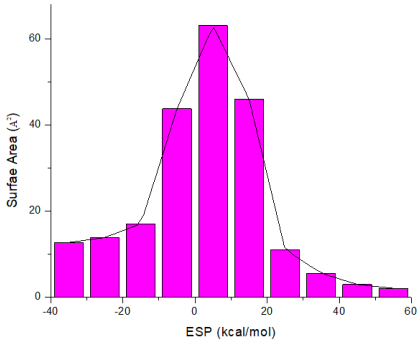

Figure 6: Histogram representing the Polar surface area as function of ESP.

3.5 NLO Analysis

The optimized structure of the 7MBC was utilized to compute NLO properties such as static dipole moment (μ), anisotropy of polarizability (Δα), mean polarizability (α). Also, the first hyperpolarizability (β) and second hyperpolarizability (γ) were both static and dynamic cases using DFT/B3LYP basis set.

The polarizability (α) and hyperpolarizability (β, γ) characterize the response of a system in an applied electric field. According to Buckingham's definitions, DFT has been used as an effective tool to comprehend the NLO behaviour[33]. The NLO Parameters of the chosen molecules were calculated by finite field approach using the relations explained previously[34] from Gaussian output using B3LYP/6-311++G(d, p) functionals. These NLO parameters were reported in Table 6-9.

From the tables, it is found that the highest value of μ is observed for the component μ_y. The calculated α_{ij} has nonzero values and is dominated by the diagonal components α_{xx} and α_{yy}. The value of β_{xxx} component of computed first order static

hyperpolarizability is found to be largest which indicates that the molecules have major component of polarizability along axial direction. This large hyperpolarizability value is directly correlated charge delocalization from donor to acceptor through π conjugated framework[35]. The value of γ mainly depends on the factors such as the extent of π-electron conjugation, substituted functional groups and dimensionality of the molecules [1]. The dominant component for the magnitude of γ is found to be γ_{xxxx} (= 11.9653×10^{-36} esu).

Urea is the perfect NLO molecule and is one of the exemplary molecules frequently considered as a threshold for comparison of the NLO properties of the molecular systems[36]. On comparing with the standard values of Urea, the dipole moments are greater by ≈3 times (μ_{urea}=1.3732 D). The average linear polarizability (α_{total}) of 7MBCis 7 times larger than that of Urea ($\alpha_{urea}=38.312\times10^{-25}$esu). Also, the average first hyperpolarizability, β_{total} showed significant increase. The value is 18 times larger than that of Urea ($\beta_{urea}=372.89\times10^{-33}$esu). These results suggest that the title compounds be attractive materials for future studies of non-linear properties.

Table 6: Components of Dipole Moment (μ) and total dipole moment(μ_{total}) of 7MBC computed using B3LYP hybrid DFT functional at 6-31+G(d,p) basis set.

Molecule	Dipole moment (μ × 10^{-18} esu)			
	μ_x	μ_y	μ_z	μ_{total}
7MBC	-2.3466	-3.3838	1.1353	4.2715

Table 7: Selected Tensor components of isotropic polarizability, average isotropic polarizability ⟨α⟩, Anisotropy of polarizability (Δα) of 7MBC computed using B3LYP hybrid DFT functional at 6-31+G(d,p) basis set.

Molecule	Static Dipole Polarizability (α × 10^{-24} esu)							
	α_{xx}	α_{yx}	α_{yy}	α_{zx}	α_{zy}	α_{zz}	$\langle\alpha\rangle = \alpha_{\parallel}$	Δα
7MBC	26.9697	1.7286	22.5956	0.1113	-0.3004	10.7027	20.0893	14.8951

Table 8:Selected tensor components of β ($\beta_X, \beta_Y, \beta_Z$), total value of β, average first hyperpolarizability ⟨β⟩ about the standard orientation, Projection of β on dipole moment (β_V), Parallel and perpendicular components of β about z-axis.

Molecule	Static First Hyperpolarizability (β ×10^{-33} esu)							
	β_X	β_Y	β_Z	β_{total}	$\langle\beta\rangle = \beta_{\parallel}$	β_V	$\beta_{\parallel}$ (z)	$\beta_{\perp}$(z)
7MBC	-6336.37	2147.89	-571.27	6714.86	976.57	1627.62	-342.76	-114.25

Table 9:Selected tensor Components of second hyperpolarizability: γ ($\gamma_X, \gamma_Y, \gamma_Z$) , total value of γ, average ⟨γ⟩, normal component of γ about the standard orientation.

Molecule	Second Hyperpolarizability (γ ×10^{-36} esu)					
	γ_x	γ_y	γ_z	γ_{total}	$\langle\gamma\rangle = \gamma_{||}$	$\gamma_{\perp}$
7MBC	11.9653	4.7687	3.4208	13.3271	20.1548	6.7183

IV. Conclusion

Herein, we present quantum chemical calculations are performed for synthesized compound: 7-methoxy-2-benzofuran-corboxylic acid. The present work is devoted to systematic DFT analysis on 7MBC. The parameters of optimized geometry are found consistent literature values for identical geometries. The slight variations in these parameters were attributed to probable intermolecular interactions. DFT calculations expediently enabled us to interpret the experimental FT-IR data by assigning the computed frequencies within the framework of the group frequencies. FMO findings disclosed an energy gap of 4.190 eV indicates high polarizability and hence expected to be soft as well as reactive. The chemical reactivity of the molecules was discoursed using FMO and DOS analysis and various GRDs were estimated.. MEP reveals that the C=O bond is the most probable site for electrophilic attack. Further, quantitative description of the MEP shows that the sites electrophilic and nucleophilic attacks both are located in carboxyl group indicating the displacement of –COOH by –OH group. The hyperpolarizability values show that the titled compounds possess considerable NLO responses, larger than that of Urea and are suitable materials for further NLO studies.

References.

[1] O. Saku, M. Saki, M. Kurokawa, K. Ikeda, T. Takizawa, N. Uesaka, Synthetic studies on selective adenosine A2A receptor antagonists: Synthesis and structure-activity relationships of novel benzofuran derivatives, Bioorganic Med. Chem. Lett. 20 (2010) 1090–1093. https://doi.org/10.1016/J.BMCL.2009.12.028.

[2] B.Y. Mane, Y.S. Agasimundin, B. Shivakumar, Synthesis of benzofuran analogs of fenamates as non steroidal antiinflammatory agents, Indian J. Chem. - Sect. B Org. Med. Chem. 49 (2010).

[3] J. Kossakowski, K. Ostrowska, Synthesis of new derivatives of 2,3-dihydro-7-benzo[b]furanol with potential pharmacological activity, Acta Pol. Pharm. - Drug Res. 63 (2006).

[4] K. Chand, Rajeshwari, A. Hiremathad, M. Singh, M.A. Santos, R.S. Keri, A review on antioxidant potential of bioactive heterocycle benzofuran: Natural and synthetic derivatives, Pharmacol. Reports. 69 (2017). https://doi.org/10.1016/j.pharep.2016.11.007.

[5] T. Oka, T. Yasusa, T. Ando, M. Watanabe, F. Yoneda, T. Ishida, J. Knoll, Enantioselective synthesis and absolute

configuration of (-)-1-(benzofuran-2-yl)-2-propylaminopentane, ((-)-BPAP), a highly potent and selective catecholaminergic activity enhancer, Bioorg. Med. Chem. 9 (2001) 1213–1219. https://doi.org/10.1016/S0968-0896(00)00341-2.

[6] T. Fukai, Y. Oku, Y. Hano, S. Terada, Antimicrobial activities of hydrophobic 2-arylbenzofurans and an isoflavone against vancomycin-resistant enterococci and methicillin-resistant Staphylococcus aureus, Planta Med. 70 (2004) 685–687. https://doi.org/10.1055/S-2004-827196.

[7] J. Kossakowski, K. Ostrowska, E. Hejchman, I. Wolska, Synthesis and structural characterization of derivatives of 2- and 3-benzo[b]furan carboxylic acids with potential cytotoxic activity, Farmaco. 60 (2005). https://doi.org/10.1016/j.farmac.2005.05.005.

[8] P. Mohr, M. Nettekoven, J.-M. Plancher, H. Richter, O. Roche, T. Takahashi, S. Taylor, Benzofuran and Benzothiophene-2-carboxylic acid amide derivatives, 2009.

[9] H. Hanumanagoud, K.M. Basavaraja, Synthesis, antibacterial, antifungal activity and DNA cleavage study of 3-(7-methoxy-benzofuran-2-yl)-5-aiy1-4H-[1,2,4]triazoles, J. Chem. Pharm. Res. 4 (2012).

[10] H. Tsuji, C. Mitsui, L. Ilies, Y. Sato, E. Nakamura, Synthesis and properties of 2,3,6,7-tetraarylbenzo[1,2-b:4,5-b′] difurans as hole-transporting material, J. Am. Chem. Soc. 129 (2007) 11902–11903. https://doi.org/10.1021/JA074365W.

[11] S.J. Kim, Y. Zhang, C. Zuniga, S. Barlow, S.R. Marder, B. Kippelen, Efficient green OLED devices with an emissive layer comprised of phosphor-doped carbazole/bis-oxadiazole side-chain polymer blends, Org. Electron. 12 (2011) 492–496. https://doi.org/10.1016/J.ORGEL.2010.12.006.

[12] F.I. Wu, P.I. Shih, C.F. Shu, Y.L. Tung, Y. Chi, Highly Efficient Light-Emitting Diodes Based on Fluorene Copolymer Consisting of Triarylamine Units in the Main Chain and Oxadiazole Pendent Groups, Macromolecules. 38 (2005) 9028–9036. https://doi.org/10.1021/MA051842R.

[13] A. Sagaama, O. Noureddine, S.A. Brandán, A.J. Jędryka, H.T. Flakus, H. Ghalla, N. Issaoui, Molecular docking studies, structural and spectroscopic properties of monomeric and dimeric species of benzofuran-carboxylic acids derivatives: DFT calculations and biological activities, Comput. Biol. Chem. 87 (2020).

[14] S.M. Hiremath, A.S. Patil, C.S. Hiremath, M. Basangouda, S.S. Khemalapure, N.R. Patil, S.B. Radder, S.J.S. Armaković, S.J.S. Armaković, Structural, spectroscopic characterization of 2-(5-methyl-1-benzofuran-3-yl) acetic acid in monomer, dimer and identification of specific reactive, drug likeness properties: Experimental and computational study, J. Mol. Struct. 1178 (2019) 1–17. https://doi.org/10.1016/j.molstruc.2018.10.007.

[15] S.M. Hiremath, Vibrational, electronic and reactivity insight on (5-chloro-benzofuran-3-yl)-acetic acid hydrazide: A Spectroscopic and DFT approach., J. Mol. Struct. 1239 (2021). https://doi.org/10.1016/j.molstruc.2021.130479.

[16] M.J. Frisch, G.W. Trucks, H.B. Schlegel, G.E. Scuseria, M.A. Robb, J.R. Cheeseman, G. Scalmani, V. Barone, B. Mennucci, G.A. Petersson, H. Nakatsuji, M. Caricato, X. Li, H.P. Hratchian, A.F. Izmaylov, J. Bloino, G. Zheng, J.L. Sonnenberg, M. Had, D.J. Fox, Gaussian 09 C.01, Gaussian, Inc. Wallingford CT. (2010).

[17] R.D. Dennington II, A. Keith,Todd, M.M. John, GaussView, Version 6.0.16, (2016) Semichem Inc., Shawnee Mission KS.

[18] M.H. Jamróz, Vibrational Energy Distribution Analysis VEDA 4, Spectrochim. Acta Part A Mol. Biomol. Spectrosc. 114 (2013).

[19] J.M.L. Martin, J. El-Yazal, J.P. François, Structure and vibrational spectrum of some polycyclic aromatic compounds studied by density functional theory. 1. Naphthalene, azulene, phenanthrene, and anthracene, J. Phys. Chem. 100 (1996). https://doi.org/10.1021/jp960598q.

[20] R.G. Parr, R.G. Pearson, Absolute Hardness: Companion Parameter to Absolute Electronegativity, J. Am. Chem. Soc. 105 (1983) 7512–7516. https://doi.org/10.1021/JA00364A005/ASSET/JA00364A005.FP.PNG_V03.

[21] R.G. Pearson, Absolute Electronegativity and Hardness: Applications to Organic Chemistry, J. Org. Chem. 54 (1989) 1423–1430. https://doi.org/10.1021/JO00267A034.

[22] K. Sharma, R. Melavanki, K.K. Sadasivuni, Quantum chemical computations and photophysical spectral features studies of two coumarin compounds, Luminescence. 35 (2020). https://doi.org/10.1002/bio.3791.

[23] S. Sarala, S.K. Geetha, S. Muthu, A. Irfan, Computational investigation, comparative approaches, molecular structural, vibrational spectral, non-covalent interaction (NCI), and electron excitations analysis of benzodiazepine derivatives, J. Mol. Model. 2021 279. 27 (2021) 1–34. https://doi.org/10.1007/S00894-021-04877-Z.

[24] S. Chandrasekhar, H.R. Deepa, R. Melavanki, M.M. Basanagouda, S. Mogurampelly, J. Thipperudrappa, Computational and spectroscopic studies of biologically active coumarin-based fluorophores, Luminescence. 36 (2021) 769–787. https://doi.org/10.1002/bio.4002.

[25] S.B. Radder, R. Melavanki, S.M. Hiremath, R. Kusanur, S.S. Khemalapure, S.C. Jeyaseelan, Synthesis, Spectroscopic (FT-IR, FT-Raman, NMR & UV-Vis), Reactive (ELF, LOL, Fukui), Drug likeness and Molecular Docking insights on novel 4-[3-(3-methoxy-phenyl)-3-oxo-propenyl]-benzonitrile by Experimental and Computational Methods, SSRN Electron. J. (2021). https://doi.org/10.2139/ssrn.3931706.

[26] C.D. Vincy, J.D.D. Tarika, X.D.D. Dexlin, A. Rathika, T.J. Beaula, Exploring the antibacterial activity of 1, 2 diaminoethane hexanedionic acid by spectroscopic, electronic, ELF, LOL, RDG analysis and molecular docking studies using DFT method, J. Mol. Struct. 1247 (2022). https://doi.org/10.1016/j.molstruc.2021.131388.

[27] J. Zhang, Libreta: Computerized Optimization and Code Synthesis for Electron Repulsion Integral Evaluation, J. Chem. Theory Comput. 14 (2018) 572–587. https://doi.org/10.1021/ACS.JCTC.7B00788/SUPPL_FILE/CT7B00788_SI_001.PDF.

[28] F.A. Bulat, A. Toro-Labbé, T. Brinck, J.S. Murray, P. Politzer, Quantitative analysis of molecular surfaces: areas, volumes, electrostatic potentials and average local ionization energies, J. Mol. Model. 2010 1611. 16 (2010) 1679–1691. https://doi.org/10.1007/S00894-010-0692-X.

[29] T. Lu, F. Chen, Quantitative analysis of molecular surface based on improved Marching Tetrahedra algorithm, J. Mol. Graph. Model. 38 (2012) 314–323. https://doi.org/10.1016/J.JMGM.2012.07.004.

[30] T. Lu, F. Chen, Multiwfn: A multifunctional wavefunction analyzer, J. Comput. Chem. 33 (2012) 580–592. https://doi.org/10.1002/JCC.22885.

[31] W. Humphrey, A. Dalke, K. Schulten, VMD: Visual molecular dynamics, J. Mol. Graph. 14 (1996). https://doi.org/10.1016/0263-7855(96)00018-5.
[32] J. Zhang, T. Lu, Efficient evaluation of electrostatic potential with computerized optimized code, Phys. Chem. Chem. Phys. 23 (2021). https://doi.org/10.1039/d1cp02805g.
[33] A.D. Buckingham, Permanent and Induced Molecular Moments and Long-Range Intermolecular Forces, (2007) 107–142. https://doi.org/10.1002/9780470143582.CH2.
[34] N.R. Sheela, S. Muthu, S. Sampathkrishnan, A.A. Al-Saadi, Normal co-ordinate analysis, molecular structural, non-linear optical, second order perturbation studies of Tizanidine by density functional theory, Spectrochim. Acta Part A Mol. Biomol. Spectrosc. 139 (2015) 189–199. https://doi.org/10.1016/j.saa.2014.11.065.
[35] S.A. Siddiqui, T. Rasheed, M. Faisal, A.K. Pandey, S.B. Khan, Electronic structure, nonlinear optical properties, and vibrational analysis of gemifloxacin by density functional theory, Spectrosc. (New York). 27 (2012) 185–206. https://doi.org/10.1155/2012/614710.
[36] B. Amul, S. Muthu, M. Raja, S. Sevvanthi, Spectral, DFT and molecular docking investigations on Etodolac, J. Mol. Struct. 1195 (2019) 747–761. https://doi.org/10.1016/j.molstruc2019.06.047.